Elementary Step Model of Ethane Oxidative Dehydrogenation on Pt-Coated Monoliths

Marylin C. Huff
Center for Catalytic Science and Technology, Dept. of Chemical Engineering, University of Delaware, Newark, DE 19716

Lanny D. Schmidt
Dept. of Chemical Engineering and Materials Science, University of Minnesota, Minneapolis, MN 55455

The oxidative dehydrogenation of ethane to ethylene over Pt-coated foam monoliths in oxygen with varying levels of nitrogen dilution has been simulated using a 24-step model of adsorption, desorption and surface reactions. Reaction parameters for these elementary steps were obtained from surface science and catalysis literature or fit to previously reported experimental data. The model agrees with the experimental data remarkably well, mimicking the selectivity and conversion trends observed experimentally with changing operating conditions. The model shows that a purely heterogeneous mechanism can be used to simulate the experimental results collected near atmospheric pressure accurately, suggesting that the mechanism we propose is sufficiently accurate to capture the main features of this reaction system. This model can also be used to examine this reaction system under conditions experimentally inaccessible. Application of this predictive ability to operation of this type of reactor under probable industrial conditions suggests that excellent ethylene yields are possible.

Introduction

Experimental background

We have found that ethylene can be produced with high yields and conversions by oxidative dehydrogenation of ethane over Pt-coated α-Al_2O_3 foam monoliths in an atmospheric-pressure reactor with contact times < 10 ms (Huff and Schmidt, 1993), and more recent experiments indicate that these yields may be obtained at contact times as short as 200 μs (Witt and Schmidt, 1996). Although thermodynamic equilibrium predicts carbon deposition and minimal ethylene production under these conditions, ethylene yields are comparable to the industrial yields of steam cracking (Song et al., 1992). However, these reaction times τ are two to three orders of magnitude smaller (lower capital cost) without the need to supply heat externally for endothermic reactions (lower production costs). Therefore, ethane oxidative dehydrogenation is a promising alternative to industrial steam cracking for the production of olefins, and its mechanism needs to be understood.

Correspondence concerning this article should be addressed to M. C. Huff.

The reactor used here is described in detail elsewhere (Huff and Schmidt, 1993). The catalyst support is a 45-ppi (pores per liner inch) α-Al_2O_3 foam monolith with a surface area of ~ 100 cm^2/g. This low surface area support has a fairly high loading of Pt (~ 5 wt. %) that leads to a thin film of Pt metal on the surface with little exposed oxide. We assumed an average pore perimeter, σ, of 0.20 cm and a cross-sectional area of flow, A, of 2.5×10^{-3} cm^2 per pore. All experiments were conducted at 1.4 atm, and we will compare the model results to those experiments conducted at total flow rates of 1 to 10 slpm, or $v_o(T_o = 298) = 20$ to 250 cm/s.

The reactor operates adiabatically at $\sim 1{,}000$°C with all of the heat supplied by the exothermic oxidation reactions. We have insulated the catalyst both radially and axially to minimize radiative heat loss from the reactor and find that the reactor operates nearly isothermally.

Experimentally, nonequilibrium C_2H_4, CO_2, and H_2O production is observed over the Pt catalyst (Huff and Schmidt, 1993). Between fuel-to-oxygen ratios of 1.0 and 2.0, CO selectivity decreases and the CO_2 selectivity increases. More H_2O

is produced than H_2, and the ethane conversion steadily decreases as the composition moves farther from the combustion stoichiometry. Ethylene selectivity decreases with increasing fuel-to-oxygen ratios for oxidation in air, but increases with increasing fuel-to-oxygen ratios for oxidation in O_2 (20% N_2). Higher reaction temperatures lead to better ethylene selectivity and greater ethane conversion.

Modeling

In this article, we extend the model for the partial oxidation of methane over Pt and Rh surfaces (Hickman and Schmidt, 1993) to the significantly more complex partial oxidation and oxidative dehydrogenation of ethane over Pt surfaces. We chose the elementary steps of the reaction mechanism to agree with those suggested in previous experimental work (Huff and Schmidt, 1993), as shown in Figure 1. Figure 1a depicts the simplified mechanism, which assumes that ethane first adsorbs dissociatively on the Pt surface; Figure 1b shows more detail with activation energy barriers for the important steps. The model allows for both straight dissociative adsorption (Eq. 1) and oxygen-assisted adsorption (Eq. 2). This mechanism combines 12 steps from the mechanism for hydrogen oxidation (Williams et al., 1992) and 6 steps from methane oxidation (Hickman and Schmidt, 1993). These rate expressions were not adjusted for these calculations.

Five additional steps to account for ethane and ethylene adsorption, desorption, and surface reactions are added to yield a 23-step surface-reaction mechanism with 36 known rate parameters (18 preexponentials and 18 activation energies) that are not adjustable. The model reactions include the steps

$$C_2H_6(g) \xrightarrow{k_{aC_2H_6}} C_2H_5 + H \qquad (1)$$

$$C_2H_6(g) + O \xrightarrow{k'_{aC_2H_6}} C_2H_5 + OH \qquad (2)$$

$$O_2(g) \underset{k_{dO}}{\overset{k_{aO}}{\rightleftharpoons}} 2O \qquad (3a,b)$$

for dissociative reactant adsorption, the steps

$$2H \underset{k_{aH}}{\overset{k_{dH}}{\rightleftharpoons}} H_2(g) \qquad (4a,b)$$

$$H_2O \underset{k_{aH_2O}}{\overset{k_{dH_2O}}{\rightleftharpoons}} H_2O(g) \qquad (5a,b)$$

$$CO \underset{k_{aCO}}{\overset{k_{dCO}}{\rightleftharpoons}} CO(g) \qquad (6a,b)$$

$$CO + O \underset{k_{aCO_2}}{\overset{k_{dCO_2}}{\rightleftharpoons}} CO_2(g) \qquad (7a,b)$$

$$C_2H_4 \xrightarrow{k_{dC_2H_4}} C_2H_4(g) \qquad (8)$$

for product desorption, and the steps

$$H + O \underset{k_{-1}}{\overset{k_1}{\rightleftharpoons}} OH \qquad (9a,b)$$

$$H + OH \underset{k_{-2}}{\overset{k_2}{\rightleftharpoons}} H_2O \qquad (10a,b)$$

$$C + O \underset{k_{-3}}{\overset{k_3}{\rightleftharpoons}} CO \qquad (11a,b)$$

$$C_2H_5 \xrightarrow{k_4} C_2H_4 + H \qquad (12)$$

$$C_2H_4 \xrightarrow{k_5} 2C + 4H \qquad (13)$$

$$2OH \underset{k_{-6}}{\overset{k_6}{\rightleftharpoons}} H_2O + O \qquad (14a,b)$$

for surface reactions. All species are surface species unless noted as gas phase (g). Most of the reactions are considered reversible except for ethane adsorption, ethyl decomposition, and ethylene desorption or decomposition. The decomposition of ethane and its fragments is considered irreversible due to the large activation energy barrier for the reverse processes. This is the basic model that will initially be discussed here. We also discuss an extended model that includes the secondary reaction of steam-reforming surface carbon,

$$C + H_2O \xrightarrow{k_7} 2H + CO. \qquad (15)$$

This reaction is not added initially because the kinetics of this reaction are unknown.

Most of the reaction-rate parameters (preexponentials and activation energies) were independently obtained experimen-

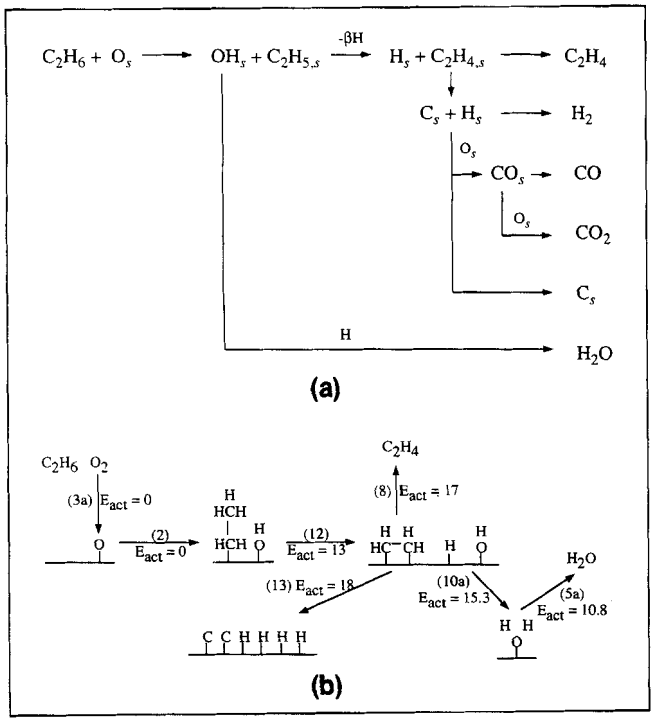

Figure 1. Proposed surface reactions in ethane oxidation.

(a) Overall reaction network: the gaseous species produced are indicated at the right. This is a simplified version of a more complete reaction mechanism (Huff and Schmidt, 1993). (b) Detail of the adsorption and decomposition of ethane reactions. The numbers in parentheses correspond to the equation number in the text for each step. The activation energy in kcal/mol is indicated for each of these steps.

tally and are reported elsewhere in the literature. The origin of these parameters is listed in Table 1 and discussed in detail in the methane oxidation model (Hickman and Schmidt, 1993).

Rate parameters for the steps involving ethane or ethane fragments are less well known. We obtained activation energies for many of these steps (Eqs. 1, 8, and 12–13) from energetic estimations (Carter and Koel, 1990). These theoretically estimated values agree well with the somewhat scattered experimental determinations (Windham et al., 1988; Ogle et al., 1986; Berlowitz et al., 1985; Gland et al., 1988; Mohsin et al., 1989; Kang and Anderson, 1985). Due to the lack of information regarding the activation energy for the oxygen-assisted adsorption step (Eq. 2), we assumed an activation energy of 0 kcal/mol.

Since the preexponentials for these reactions are unknown, they are treated as adjustable parameters, the only adjustable parameters in the basic, 23-step model. Thus, in the basic model, we consider 18 activation energies as given, obtain four activation energies from estimations, and use an educated guess for the final activation energy. Likewise, we consider 18 of the 23 preexponentials as given and adjust the remaining 5 to obtain an accurate fit of the data. The extended model has two additional adjustable parameters, the preexponential and activation energy for steam reforming of carbon (Eq. 15). All of the rate parameters used in both models are listed in Table 1.

Mass-Transfer Limitations

In this model, we have not explicitly incorporated mass transfer from the bulk to the surface through the boundary layer and back to the bulk. The methane oxidation model (Hickman and Schmidt, 1993) did account for the possibility

Table 1. Rate Parameters

Reaction	k_o (s^{-1} or $torr^{-1}\cdot s^{-1}$)	E_a (kcal/mol)	Reference
$C_2H_6(g) \xrightarrow{k_{aC_2H_6}} C_2H_5 + H$	4.9×10^{4}	4	This work (Carter and Koel, 1990)
$C_2H_6(g) \xrightarrow{k'_{aC_2H_6}} C_2H_5 + OH$	3.8×10^{5}	0	This work
$O_2(g) \xrightarrow{k_{aO}} 2O$	1.0×10^{4}	0	(Hickman and Schmidt, 1993)
$2O \xrightarrow{k_{dO}} O_2(g)$	1.0×10^{13}	52	(Matsushima, 1985)
$2H \xrightarrow{k_{dH}} H_2(g)$	1.0×10^{13}	18	(McCabe and Schmidt, 1977)
$H_2(g) \xrightarrow{k_{aH}} 2H$	7.5×10^{4}	0	(Williams et al., 1992)
$H_2O \xrightarrow{k_{dH_2O}} H_2O(g)$	1.0×10^{13}	10.8	(Fisher and Gland, 1977)
$H_2O(g) \xrightarrow{k_{aH_2O}} H_2O$	5.0×10^{4}	0	(Williams et al., 1992)
$CO \xrightarrow{k_{dCO}} CO(g)$	1.0×10^{14}	30	(McCabe and Schmidt, 1977)
$CO(g) \xrightarrow{k_{aCO}} CO$	3.2×10^{5}	0	(Campbell et al., 1981)
$CO + O \xrightarrow{k_{dCO_2}} CO_2(g)$	1.0×10^{14}	24.1	(Campbell et al., 1980)
$CO_2(g) \xrightarrow{k_{aCO_2}} CO + O$	3.2×10^{5}	36	(Hickman and Schmidt, 1993)
$C_2H_4 \xrightarrow{k_{dC_2H_4}} C_2H_4(g)$	1.6×10^{13}	17	This work (Carter and Koel, 1990)
$H + O \xrightarrow{k_1} OH$	1.0×10^{15}	2.5	(Williams et al., 1992)
$OH \xrightarrow{k_{-1}} O + H$	1.0×10^{8}	5.0	(Williams et al., 1992)
$H + OH \xrightarrow{k_2} H_2O$	9.0×10^{16}	15.3	(Williams et al., 1992)
$H_2O \xrightarrow{k_{-2}} H + OH$	1.8×10^{13}	36.8	(Williams et al., 1992)
$C + O \xrightarrow{k_3} CO$	5.0×10^{13}	15	(Hickman and Schmidt, 1993)
$CO \xrightarrow{k_{-3}} C + O$	1.0×10^{11}	44	(Hickman and Schmidt, 1993)
$C_2H_5 \xrightarrow{k_4} C_2H_4 + H$	1.0×10^{13}	13	This work (Carter and Koel, 1990)
$C_2H_4 \xrightarrow{k_5} 2C + 4H$	3.3×10^{13}	18	This work (Carter and Koel, 1990)
$2OH \xrightarrow{k_6} H_2O + O$	1.0×10^{15}	12.3	(Fisher and Gland, 1977)
$H_2O + O \xrightarrow{k_{-6}} 2OH$	1.0×10^{15}	31	(Hickman and Schmidt, 1993)
$C + H_2O \xrightarrow{k_7} CO + 2H$	1.0×10^{13}	16.9	This work

of mass-transfer limitations. Hickman and Schmidt showed that for coefficients of mass transfer, k_m, greater than 1,000 cm/s, the reaction rates and product distribution are independent of the mass-transfer rate. Hence, for $k_m > 1{,}000$ cm/s, the system is reaction limited. However, since the surface reactions are very fast compared to the gas-phase adsorption steps, the rates are limited by the flux of C_2H_6 and/or O_2 to the surface. Thus, the rates of the dissociative adsorption steps have been set at the flux limit to account for the mass-transfer limitation.

Basic Model

The model described here is an initial-value differential equation problem that uses the shooting method to solve a one-dimensional lumped-parameter model of a tube-wall reactor. The tortuous, multiply connected paths of the pores within the foam monolith are approximated as straight, cylindrical channels with an average effective pore diameter of 1 mm and a void fraction of 0.8. This approximation is discussed in more detail in a later section.

The model assumes isothermal operation. Experimentally, this monolithic type of reactor operates very nearly isothermally at the adiabatic reaction temperature with little heat loss. The model mimics this behavior.

The model solves for the steady-state coverages of all species, θ_i, at incremental steps along the length of the catalyst for a given temperature. From these coverages, gas-phase partial pressures, P_i, and production rates, r_i, for each gas-phase species are determined for each incremental step. Final reactant conversions and product selectivities are calculated at the reactor exit.

Surface-species mass balances

In the model, we calculate steady-state coverages for all species at incremental steps along the length of the catalyst according to the expressions

$$\frac{d\theta_{CO}}{dt} = 0 = k_{aCO} P_{CO} \theta_v - k_{dCO} \theta_{CO} + k_{aCO_2} P_{CO_2} \theta_v - k_{dCO_2} \theta_{CO} \theta_O + k_3 \theta_C \theta_O - k_{-3} \theta_{CO} \theta_v \quad (16)$$

$$\frac{d\theta_{H_2O}}{dt} = 0 = k_{aH_2O} P_{H_2O} \theta_v - k_{dH_2O} \theta_{H_2O} + k_2 \theta_H \theta_{OH} - k_{-2} \theta_{H_2O} \theta_v + k_6 \theta_{OH}^2 - k_{-6} \theta_{H_2O} \theta_O \quad (17)$$

$$\frac{d\theta_{OH}}{dt} = 0 = k'_{aC_2H_6} P_{C_2H_6} \theta_O \theta_v + k_1 \theta_H \theta_O - k_{-1} \theta_{OH} \theta_v - k_2 \theta_H \theta_{OH} + k_{-2} \theta_{H_2O} \theta_v - 2k_6 \theta_{OH}^2 + 2k_{-6} \theta_{H_2O} \theta_O \quad (18)$$

$$\frac{d\theta_O}{dt} = 0 = -k'_{aC_2H_6} P_{C_2H_6} \theta_O \theta_v + 2k_{aO} P_{O_2} \theta_v - k_{dO} \theta_O^2 + k_{aCO_2} P_{CO_2} \theta_v - k_{dCO_2} \theta_{CO} \theta_O - k_1 \theta_H \theta_O + k_{-1} \theta_{OH} \theta_v - k_3 \theta_C \theta_O + k_{-3} \theta_{CO} \theta_v + k_6 \theta_{OH}^2 - k_{-6} \theta_{H_2O} \theta_O \quad (19)$$

$$\frac{d\theta_H}{dt} = 0 = k_{aC_2H_6} P_{C_2H_6} \theta_v + 2k_{aH} P_{H_2} \theta_v - 2k_{dH} \theta_H^2 - k_1 \theta_H \theta_O + k_{-1} \theta_{OH} \theta_v - k_2 \theta_H \theta_{OH} + k_{-2} \theta_{H_2O} \theta_v + k_4 \theta_{C_2H_5} \theta_v + 4k_5 \theta_{C_2H_4} \theta_v \quad (20)$$

$$\frac{d\theta_C}{dt} = 0 = -k_3 \theta_C \theta_O + k_{-3} \theta_{CO} \theta_v + 2k_5 \theta_{C_2H_4} \theta_v \quad (21)$$

$$\frac{d\theta_{C_2H_4}}{dt} = 0 = -k_{dC_2H_4} \theta_{C_2H_4} + k_4 \theta_{C_2H_5} \theta_v - k_5 \theta_{C_2H_4} \theta_v \quad (22)$$

$$\frac{d\theta_{C_2H_5}}{dt} = 0 = k_{aC_2H_6} P_{C_2H_6} \theta_v + k'_{aC_2H_6} P_{C_2H_6} \theta_O \theta_v - k_4 \theta_{C_2H_5} \theta_v, \quad (23)$$

where θ_i are fractional surface coverages and θ_v is the fraction of surface sites that are vacant ($\theta_v = 1 - \Sigma\theta_i$). These equations include all of the steps previously listed (Eqs. 1–14). We used the assumption made in the methane model (Hickman and Schmidt, 1993) that all species adsorb competitively on the Pt surface and coverages greater than one monolayer do not occur.

We made several assumptions regarding the order of some of the steps. We assumed first-order adsorption and desorption of H_2 and O_2, which is in agreement with the assumptions made in the methane model. Secondly, we assumed that all adsorption and surface reaction steps require at most one vacant site. This assumption can be rationalized by the understanding that although the surface coverage may be fairly high, there is a rapid turnover at each adsorption site. A reaction that stoichiometrically requires several vacant sites, for example, ethylene decomposition to C and H (Eq. 13), actually takes place sequentially and only requires one vacant site at a time. This assumption is discussed in more detail later in this article.

Model equations

In this plug-flow tubular-reactor model (PFR), we integrate these coupled species balances along the length of the tube to satisfy the differential mass balances:

$$\frac{d(FP_i)}{dz} = \frac{\sigma F_o R_g T_o}{A v_o N_{av}} \sum_j \nu_{ij} r_j, \quad (24)$$

where the variables are defined in the Notation section at the end of this article. A complete derivation of Eq. 24 is given in the methane oxidation model (Hickman and Schmidt, 1993).

The total molar flow rate is allowed to vary as the number of moles changes due to reaction through the equation

$$\frac{dF}{dz} = \frac{\sigma}{N_{av}} \sum_i r_i. \quad (25)$$

Thus, the total molar flow rate is an additional variable in the integration along the length of the catalyst. In the model

we simultaneously integrate Eqs. 24 and 25 subject to the species balance constraints Eqs. 16–23.

In Eqs. 24 and 25, the rates, r_i, are the rates of formation of the gas-phase species. These rates are given by:

$$r_{C_2H_6} = -k_{aC_2H_6}P_{C_2H_6}\theta_v - k'_{aC_2H_6}P_{C_2H_6}\theta_O\theta_v \quad (26)$$

$$r_{O_2} = -k_{aO}P_{O_2}\theta_v + k_{dO}\theta_O^2 \quad (27)$$

$$r_{H_2} = k_{dH}\theta_H^2 - k_{aH}P_{H_2}\theta_v \quad (28)$$

$$r_{CO_2} = k_{dCO_2}\theta_{CO}\theta_O - k_{aCO_2}P_{CO_2}\theta_v \quad (29)$$

$$r_{CO} = k_{dCO}\theta_{CO} - k_{aCO}P_{CO}\theta_v \quad (30)$$

$$r_{H_2O} = k_{dH_2O}\theta_{H_2O} - k_{aH_2O}P_{H_2O}\theta_v \quad (31)$$

$$r_{C_2H_4} = k_{dC_2H_4}\theta_{C_2H_4} \quad (32)$$

based on the reactions listed in Eqs. 1–14.

Energy balance

We assume that the gas-phase temperature equilibrates with the catalyst temperature ($T_g = T_s$) and that the reactor is adiabatic. This autothermal reaction temperature is a function of the heat generated by reaction and heat input with the reactants. Ignoring thermal conduction, this energy balance can be expressed as

$$C_p(T_c - T_o) = \sum_i (-H_i)X_i, \quad (33)$$

or, alternatively, as

$$\sum_i F_{io}\left(\Delta H^o_{f,298} + \int_{298}^{T_o} C_p\, dT\right) = \sum_i F_i\left(\Delta H^o_{f,298} + \int_{298}^{T_g} C_p\, dT\right), \quad (34)$$

where the lefthand side and righthand side are the heat content of the reactants and products, respectively. This balance neglects all heat losses (adiabatic). Thermodynamic information is listed in Table 2.

Conversion and selectivity

Conversion and selectivities are calculated from the model results in the same way that the conversion and selectivities were calculated experimentally (Huff and Schmidt, 1993). The oxygen is always completely consumed in the experiments, so the conversion is an ethane conversion calculated on a carbon atom basis:

$$C = \frac{2F_{C_2H_4} + F_{CO} + F_{CO_2}}{2F_{C_2H_6} + 2F_{C_2H_4} + F_{CO} + F_{CO_2}} \times 100, \quad (35)$$

where F_i is the molar flow rate of species i. Likewise, the selectivities to C_2H_4, CO, and CO_2 are calculated on a carbon atom basis:

$$S_{C_2H_4} = \frac{2F_{C_2H_4}}{2F_{C_2H_4} + F_{CO} + F_{CO_2}} \times 100 \quad (36)$$

$$S_{CO} = \frac{F_{CO}}{2F_{C_2H_4} + F_{CO} + F_{CO_2}} \times 100 \quad (37)$$

$$S_{CO_2} = \frac{F_{CO_2}}{2F_{C_2H_4} + F_{CO} + F_{CO_2}} \times 100. \quad (38)$$

The hydrogen and water selectivities are calculated on a hydrogen atom basis:

$$S_{H_2} = \frac{2F_{H_2}}{4F_{C_2H_4} + 2F_{H_2} + 2F_{H_2O}} \times 100 \quad (39)$$

$$S_{H_2O} = \frac{2F_{H_2O}}{4F_{C_2H_4} + 2F_{H_2} + 2F_{H_2O}} \times 100. \quad (40)$$

Although these definitions are comparable to the definitions used experimentally, the model allows for a much smaller set of possible products. For example, the model does not allow for the production of CH_4 and C_4H_8 that are typically present with selectivities $< 7\%$ and $< 3\%$, respectively (Huff and Schmidt, 1993). We chose to eliminate CH_4 and C_4H_8 from the model for two reasons: (1) kinetic parameters for the required reactions were not available, and (2) our main focus was the competition between olefin and syngas formation. Inclusion of CH_4 and C_4H_8 would cloud this issue. However, without CH_4 and C_4H_8 production, the model cannot exactly simulate experimental results. The variation between experimental data and model predictions is more apparent in the hydrogen atom selectivities (Eqs. 39 and 40) since the dominant excluded products (CH_4 and C_4H_8) contain significant amounts of hydrogen.

Table 2. Heat Capacities and Heats of Formation

	C_p (J/mol·K) $= A + BT + CT^2 + DT^3 + ET^4$					$\Delta H^o_{f,298}$
	A	$10^3\ B$	$10^5\ C$	$10^8\ D$	$10^{11}\ E$	kJ/mol
C_2H_6	33.8339	−11.5175	37.6892	−41.1770	13.8890	−83.82
O_2	29.8832	−11.3842	4.33779	−3.70082	1.01006	0.00
CO	29.0063	2.49235	−1.86440	4.79892	−2.87266	−110.525
H_2	17.9386	67.0055	−13.1485	10.5883	−2.91803	0.00
H_2O	34.0471	−9.65064	3.29983	−2.04467	0.430228	−241.818
C_2H_4	16.8346	51.5193	21.6352	−34.5618	15.87794	52.51
N_2	29.4119	−3.00681	0.545064	0.513186	−0.425308	0.00
CO_2	19.0223	79.6291	−7.37067	3.74572	−0.813304	−393.509

Extended Model

The extended, 24-step model is identical to the basic model with the addition of steam reforming of carbon (Eq. 15). The only other route to remove carbon from the surface is by CO formation, which may go on to CO_2 and requires the presence of oxygen. Conversely, the steam-reforming reaction is a secondary reaction that can lead to changes in the product distribution after the reactants (C_2H_6 and O_2) have been consumed.

The surface species mass balances in this version of the model parallel the mass balances for the basic model (Eqs. 16–23) with an additional term in the C, H_2O, CO, and H balances to account for the contribution of the steam-reforming reaction (Eq. 15). The remainder of the model equations and calculations are unchanged.

Variations with Position along the Reactor

Experimentally, we are only able to measure the entrance and exit gas-phase composition in the reaction. There is no *in situ* experimental way to probe the surface coverages of the adsorbed species or the gas-phase partial pressures predicted along the length of the catalyst. In our model, however, we calculate these values continuously. The following subsections discuss profiles of surface coverages and partial pressures along the length of the catalyst for ethane oxidation in O_2.

Surface coverages

The fractional coverages of all surface species are shown in Figure 2a as a function of position in the catalyst pore. The dominant surface species are C and CO. All other surface species have fractional coverages less than 10^{-3} monolayers. The catalyst surface very quickly acquires nearly a full monolayer coverage of carbon that blocks Pt sites and reduces the catalyst activity. Although low activity catalysts are usually avoided, in this case the reduction in active sites prevents the complete decomposition of the ethyl group to C and H atoms and increases the selectivity to C_2H_4.

Partial pressures

The corresponding gas-phase partial pressures are shown in Figure 2b as a function of position along the catalyst pore. The partial pressures of C_2H_6 and O_2 decrease rapidly along the length of the catalyst, resulting in the high conversions seen in the simulations and in the experiments. The model does not predict the complete O_2 consumption that is obtained experimentally (Huff and Schmidt, 1993), but rather about 90% O_2 conversion. This variation between the data and the model may be partially attributed to the assumption made regarding the length of the catalyst pore relative to the physical length of the monolith. This is discussed in detail in the next subsection.

Near the catalyst exit the partial pressures of CO and H_2 begin to increase more rapidly as the partial pressure of H_2O begins to drop. Likewise, the surface coverages of CO and H increase as the coverage of C decreases. In this portion of the reactor the steam reforming of carbon reaction (Eq. 15) is having a significant effect on the product distribution. Adsorbed H_2O reacts with the abundance of carbon on the surface to form CO and H that relatively quickly desorb as CO and H_2 and make additional surface sites available for the adsorption of gas-phase species. Gas-phase H_2O adsorbs on these vacant sites, producing a net increase in H_2O coverage even though H_2O is consumed by the surface reaction.

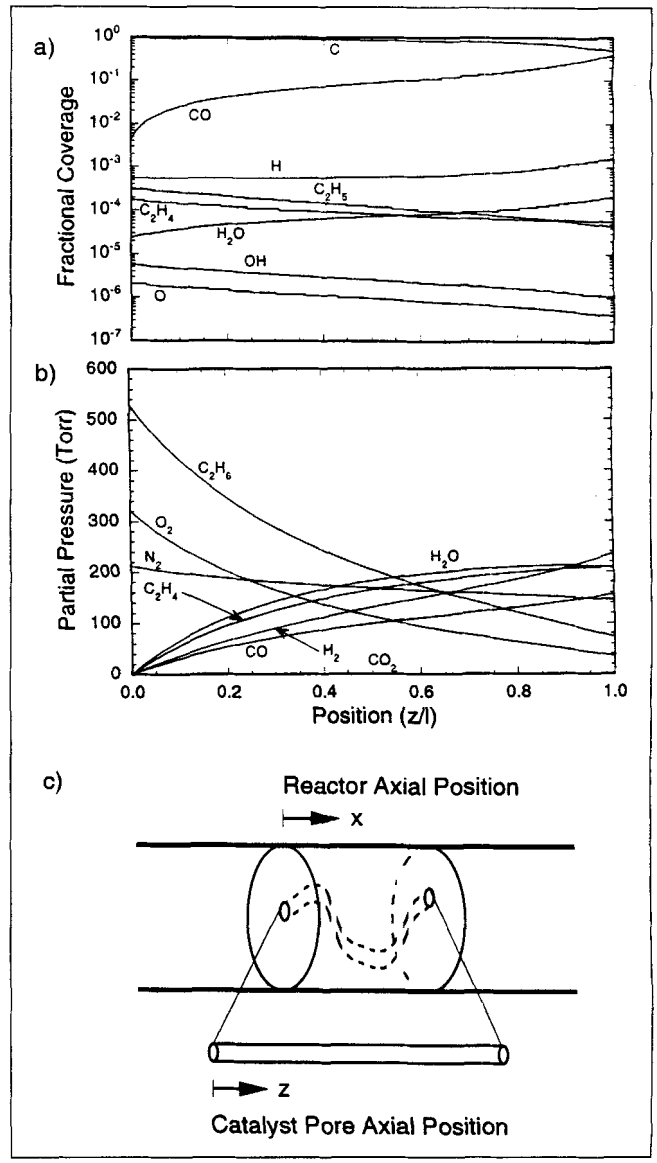

Figure 2. Surface- and gas-phase species concentrations predicted by the extended model as a function or position in the monolith.

(a) Fractional surface coverages of adsorbed species. (b) Gas phase partial pressures of reactants and products. The curves are model predictions for ethane oxidation in O_2 (20% N_2) at a C_2H_6/O_2 ratio of 1.65 at a total flow rate of 5 slpm at a reactor pressure of 1.4 atm and temperature of 900°C. (c) Experimentally, the monolith is 1 cm in length. Because of the tortuosity of the pores, this corresponds to a longer length for an individual pore.

Position

As shown in Figure 2c, there is a distinction between position within the catalyst and position within the catalyst pore.

The monolithic catalyst has some physical, bulk dimensions. All experiments (Huff and Schmidt, 1993) were conducted using monoliths 18 mm in diameter by 1 cm in length. The model, however, uses the dimensions of an individual macropore in the monolith. These pores have an average pore diameter given by the manufacturer, but the average axial length of the pores is unknown. Depending on the tortuosity of the pores, this length is approximately one to five times the physical length of the monolith.

When comparing the model predictions to the experimental results, we assume that the catalyst pore length is equal to the length of the monolith. This most certainly underestimates the available surface area, but it also underestimates the gas-phase velocity through the pore. These two effects balance each other to some extent and reduce the potential error of the equal-length assumption. Considering the number of other assumptions and approximations made in this model, this is a minor point.

Model vs. Experiments

Ethane oxidation in air

Figure 3 shows the experimental data and model predictions for ethane oxidation in air as a function of the fuel-to-oxygen ratio in the feed. The data presented are recent experimental results (Huff and Schmidt, 1993; Witt and Schmidt, 1996).

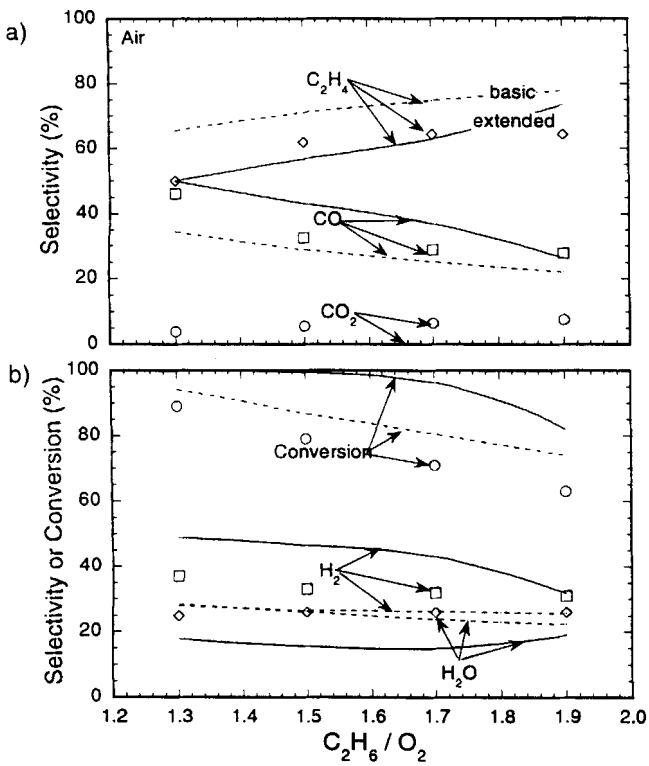

Figure 3. Selectivity and conversion for ethane oxidation in air over a 45-ppi 4.7-wt. % Pt catalyst as a function of reactant composition.

The experimental data were collected at 1.4 atm with a total flow rate of 5 slpm. The points are experimental data, the dashed curves are the predictions of the basic model, and the solid curves are the predictions of the extended model.

With the basic model, we predict the trends in selectivities and ethane conversion. The rates for C_2H_6 adsorption ($k_{aC_2H_{6,o}}$ and $k'_{aC_2H_{6,o}}$), C_2H_4 desorption ($k_{dC_2H_{4,o}}$), and the decomposition of C_2 fragments ($k_{4,o}$ and $k_{5,o}$) were adjusted to "tune" the conversion and selectivities to the experimental values at a C_2:O_2 ratio of 1.65. The model predicts a selectivity to C_2H_4 greater than experimentally observed and predicts virtually no CO_2 formation, but agrees well with the CO and H_2O selectivity, especially at the higher C_2:O_2 ratios. The basic model captures the selectivity trends remarkably well, except the CO selectivity at low fuel-to-oxygen ratios where experimentally the adiabatic reaction proceeds much faster at a much higher initial temperature such that temperature gradient develops along the length of the catalyst and the isothermal operation assumption fails.

The basic model is unable to match all of the selectivity data since the model does not allow for the production of CH_4 (up to 7%) or C_4H_8 (up to 3%), which are observed experimentally. These reactions are not included in the model because their kinetics are unknown and would only serve to increase the number of adjustable parameters. The limited species in the model also affects our ability to predict both the H_2 and H_2O selectivities accurately, but the model agrees quite well with the experimental results for these species. The model and data show decreasing H_2 and H_2O selectivities at higher fuel-to-oxygen ratios. The basic model accurately predicts the ethane conversion at all compositions, but with a slightly slower conversion loss than is seen experimentally.

The extended model predictions are also shown in Figure 3 (solid curves). The preexponential and activation energy for the steam reforming of carbon (Eq. 15) were adjusted to obtain an optimum fit of the data. The inclusion of this additional step leads to a more accurate depiction of the C_2H_4 selectivity at the expense of the accuracy of the conversion and H_2O selectivity predictions. Agreement with the other species also changes, but not as dramatically as these. The extended model predicts a break in the selectivities and conversion at a fuel-to-oxygen ratio of ~ 1.7. This corresponds to the point at which complete oxygen conversion is obtained and no gas-phase oxygen is present in the product distribution.

Nitrogen dilution

Figure 4 shows a comparison of experimental data and the model predictions for ethane oxidation at a fixed fuel-to-oxygen ratio of 1.0 as a function of the level of N_2 dilution. Figure 4 shows experimental data points, the basic model predictions (dashed lines), and the extended model predictions (solid lines). We note that the rate parameters were not adjusted from the values used for the fits shown in Figure 3 and listed in Table 1.

With both the basic and the extended models, we are able to predict the experimental data remarkably well. However, the two models show opposite trends for C_2H_4, CO, H_2, and H_2O selectivity with the level of dilution. With only three experimental data points, it is difficult to judge the relative value of the models, but the extended model (solid curves) is somewhat more quantitatively accurate. At this low fuel-to-oxygen ratio, CO and H_2 are the dominant products experimentally, while the basic model predicts more C_2H_4 and H_2O

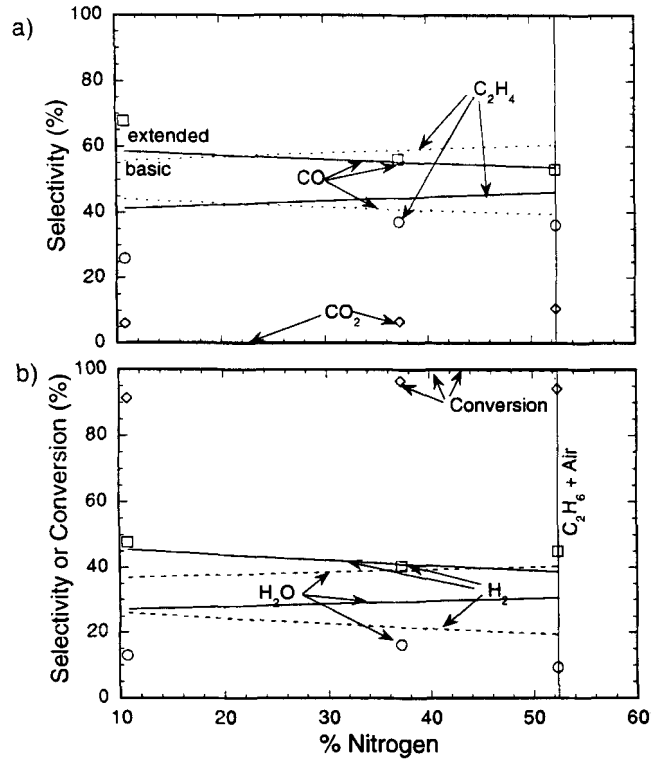

Figure 4. Selectivity and conversion for ethane oxidation over a 45-ppi 4.7-wt. % Pt catalyst as a function of the level of N_2 dilution at a fuel to O_2 ratio of 1.0.

The experimental data were collected at 1.4 atm with a total flow rate of 2.5 slpm. The points are experimental data, the dashed curves are the predictions of the basic model, and the solid curves are the predictions of the extended model.

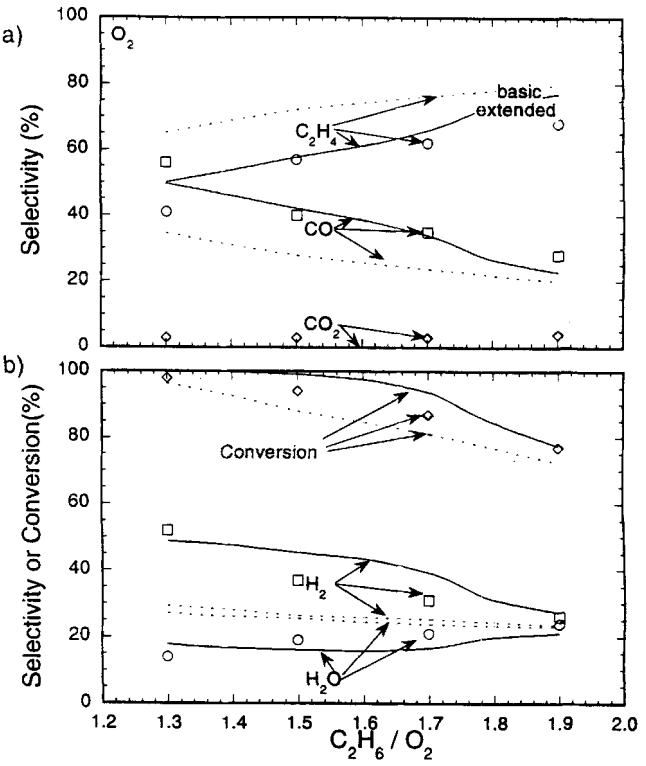

Figure 5. Selectivity and conversion for ethane oxidation in O_2 (20% N_2 dilution) over a 45-ppi 4.7-wt. % Pt catalyst as a function of reactant composition.

The experimental data were collected at 1.4 atm with a total flow rate of 4.5 slpm. The points are experimental data, the dashed curves are the predictions of the basic model, and the solid curves are the predictions of the extended model.

than is observed. In the extended model, the addition of a single reaction (Eq. 15) to the model results in a shift in product prediction to CO and H_2, which agrees well with the experimental data.

Ethane oxidation in oxygen

Figure 5 compares the experimental data, basic model predictions (dashed curves), and extended model predictions (solid curves) for ethane oxidation in O_2. In these experiments, 20% nitrogen was added to the feed for GC calibration.

As in Figure 3 for ethane oxidation in air, in Figure 5, the basic model accurately predicts the selectivity trends with fuel-to-oxygen ratio. As before, the basic model predicts more C_2H_4 formation than CO. It is important to recall that the model does not allow for any reactions leading to C_2H_4 loss such as oxidation

$$C_2H_4 + O_2 \rightarrow 2CO + 2H_2, \tag{41}$$

which will lead to CO formation, or dimerization,

$$2C_2H_4 \rightarrow C_4H_8. \tag{42}$$

In light of these simplifications, we are able to make excellent predictions using this model.

However, the basic model does not predict accurately the shapes of the H_2 and H_2O selectivities. The model predicts nearly constant selectivities to H_2 and H_2O at about 25%, while experimentally we observe more H_2 and less H_2O at the lower fuel-to-oxygen ratios. However, the basic model neglects the possibility of steam-reforming reactions including steam reforming of carbon (Eq. 15) and steam reforming of C_2H_4,

$$C_2H_4 + 2H_2O \rightarrow 2CO + 4H_2, \tag{43}$$

which may be quite important at the low fuel-to-oxygen ratios where the O_2 is quickly depleted, leaving high relative concentrations of C_2H_4 and H_2O.

The extended model tracks all of the selectivities and conversion much more closely than the basic model. By including steam reforming of carbon, this model more accurately reflects the data, particularly at low fuel-to-oxygen ratios where the basic model was least accurate. As seen previously, the extended model predicts a break in the selectivity and conversion trends at a fuel-to-oxygen ratio of ~ 1.7 that corresponds to complete oxygen conversion under these conditions.

Parameter Sensitivities

The goal of this model is to expand the elementary step model proposed for methane oxidation (Hickman and Schmidt, 1993) using the steps proposed experimentally (Huff and Schmidt, 1993) to predict the observed products on Pt surfaces accurately. In the previous section, we showed that this could be done. Many of the rate parameters needed for this model were obtained from independent sources, but unfortunately, not all of the required rate parameters have been independently measured. In several cases (noted in Table 1), activation energies for the reactions were known, but preexponentials were not.

Since some of the parameters used in this model are essentially adjustable because they are unknown, it is important to understand how changes in their values affect the model results. Analyses of the sensitivity of the model to slight changes in the values of the preexponentials for the "adjustable" rates are shown in Table 3. Sensitivities are defined as

$$S_{k,i} = \frac{\Delta x/x}{\Delta k_i/k_{i,o}} \times 100, \tag{44}$$

where x is the model output variable of interest ($S_{C_2H_4}$, S_{CO}, S_{H_2}, or conversion). This exercise helps to determine which reaction steps are the most important in determining the selectivities and conversion. In some cases the value of the rate parameter has little effect on the model results, but in other cases the effect can be quite large. In all cases the sensitivities correspond to the extended model.

$C_2H_6(g) \rightarrow C_2H_5 + H$

The intuitively obvious first step in this mechanism is molecular adsorption of ethane,

$$C_2H_6(g) \rightarrow C_2H_6. \tag{45}$$

However, the subsequent hydrogen removal on the surface

$$C_2H_6 \rightarrow C_2H_5 + H \tag{46}$$

is fast relative to the adsorption step, resulting in a lumped adsorption–decomposition step. Therefore, we lump these steps as $C_2H_6(g) \rightarrow C_2H_5 + H$. The model is obviously sensitive to the value of the rate of this reaction, suggesting that this lumped step is quite important.

Table 3. Model Sensitivities to Changes in the Rates of the Various Reaction Steps for Ethane Oxidation in O_2 (20% N_2) at a Fuel-to-Oxygen Ratio of 1.65 with a Total Flow Rate of 5 slpm at a Reaction Temperature of 900°C

Reaction	$S_{C_2H_4}$	S_{CO}	S_{H_2}	Conversion
$C_2H_6(g) \xrightarrow{k_{aC_2H_6}} C_2H_5 + H$	26	−70	−38	1.2
$C_2H_6(g) + O \xrightarrow{k'_{aC_2H_6}} C_2H_5 + OH$	(+)	(−)	(−)	(+)
$C_2H_5 \xrightarrow{k_4} C_2H_4 + H$	(−)	(+)	(+)	(+)
$C_2H_4 \xrightarrow{k_{dC_2H_4}} C_2H_4(g)$	−22	58	92	51
$C_2H_4 \xrightarrow{k_5} 2C + 4H$	21	−57	−90	−52
$C + H_2O \xrightarrow{k_7} CO + 2H$	−20	53	76	22

(+) Small positive sensitivity of less than 1%.
(−) Small negative sensitivity of less than 1%.

$C_2H_6(g) + O \rightarrow C_2H_5 + OH$

This oxygen-assisted C_2H_6 dissociative-adsorption step may appear to be a lumping of C_2H_6 dissociative adsorption (Eq. 1) and surface hydroxyl formation (Eq. 9). Unlike $C_2H_6(g) \rightarrow C_2H_5 + H$ discussed earlier, the model is not significantly sensitive to the value of this rate. However, ethyl groups must adsorb on the surface by one of these two mechanisms. This model sets the sum of the rates of these two reactions at the flux limit, so changes to the two preexponentials cannot occur independently.

The first efforts at simulating this reaction system were conducted neglecting this oxygen-assisted reaction. Without the simultaneous production of C_2H_5 and OH, we were unable to achieve the high production rate of H_2O that is observed experimentally. After adding this reaction step to the mechanism in the model, we were able to match the experimental data by adjusting the preexponentials of these steps to reflect their relative importance (as shown in Table 1, $k_{aC_2H_{6,o}} = 4.9 \times 10^4$ for dissociative adsorption and $k'_{aC_2H_{6,o}} = 3.8 \times 10^5$ for oxygen-assisted dissociative adsorption), suggesting that oxygen, assisted dissociative adsorption of C_2H_6 is dominant. However, we cannot eliminate the unassisted adsorption reaction from the mechanism in the model without adversely affecting our ability to match experimental data, particularly at higher fuel-to-oxygen ratios where the oxygen coverage is somewhat lower.

$C_2H_5 \rightarrow C_2H_4 + H$

Hydrogen abstraction by the catalyst surface is the simplest way for C_2H_4 to be formed from C_2H_5. The model is insensitive to the value of the rate for this reaction step, suggesting that this step is not rate limiting, and this step can be lumped into the subsequent steps without losing accuracy:

$$C_2H_5 \rightarrow 2C + 5H \tag{47}$$

$$C_2H_5 \rightarrow C_2H_4(g) + H. \tag{48}$$

We opted not to add these lumped steps to maintain the elementary nature of the model. Of course, H may be abstracted from C_2H_5 by surface O or OH as well. Although these steps are not considered explicitly as independent reaction steps, they are accounted for through the reactions or O, H, and OH.

$C_2H_4 \rightarrow C_2H_4(g)$

This is the desired C_2H_4 production step. The model sensitivity to this ratio is counterintuitive. Increasing the rate of desorption of C_2H_4 frees surface sites for the decomposition of C_2H_4 to C and H such that it increases the rate of CO and H_2 production more than it increases the rate of C_2H_4 production.

$C_2H_4 \rightarrow 2C + 4H$

This reaction refers to the complete pyrolysis of adsorbed ethylene. It is essentially a lumping of sequential rearrange-

ment and dissociation steps (Carter and Koel, 1990), most likely going through ethylidene and ethylidyne. These steps are depicted in Figure 6. The activation energy for the first step shown, ethylidene formation, is 18 kcal/mol. The subsequent steps have activation energies ranging from ≤ 18 kcal/mol to > 30 kcal/mol. Many of these activation energy barriers are known to be coverage dependent, and all were obtained in the absence of oxygen. In this model, we lump all of the subsequent decomposition steps into the ethylidene-formation step, assuming that the presence of oxygen greatly enhances the rate of the decomposition steps. As a result, we assume that once ethylidene is formed, it has no choice but to decompose completely to C and H, which then go on to form CO, CO_2, H_2, and H_2O or accumulate on the surface.

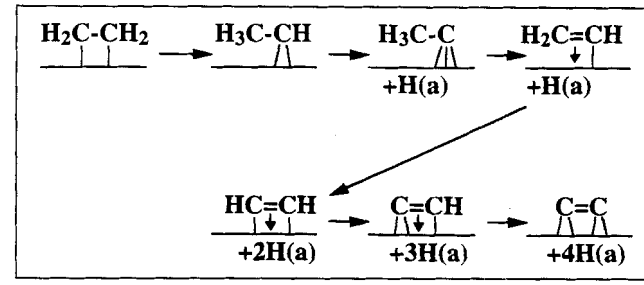

Figure 6. Energetics and mechanism for ethylene decomposition on a clean Pt surface (Carter and Koel, 1990).

$$C + H_2O \rightarrow C + 2H$$

This is the steam reforming of carbon reaction that is only present in the extended model. The model is very sensitive to the rate of this reaction, which agrees with the differences observed between the basic and the extended models. Increasing k_7 increases the conversion by removing carbon from the surface to produce a more active catalyst. Likewise, the selectivities to CO and H_2 increase. As the rate increases, the selectivity to C_2H_4 decreases, since the increased availability of vacant sites increases the rate of decomposition of C_2H_4.

Potential Energy Surface

From the activation energies listed in Table 1 and from known heats of adsorption of known species on the Pt surface, a potential energy diagram can be constructed for ethane oxidation on Pt, as shown in Figure 7. To simplify the stoichiometry throughout the diagram, a C_2H_6:O_2 ratio of 2:1 (the stoichiometric composition for oxidative dehydrogenation) was used. The right portion of Figure 7 is the ethylene-formation branch and the left portion is the syngas-formation branch. Most of the reactions in the model are depicted in this diagram, but some reactions have been eliminated to simplify the diagram.

As shown in Figure 7, ethane and oxygen dissociatively adsorb on the Pt surface. A hydroxyl group may (Eq. 2) or may not (Eq. 1) be immediately formed. The small activation energy barrier (2.5 kcal/mol) for hydroxyl formation leads to rapid additional OH production if OH is not directly formed during the adsorption step. The propensity for H_2O production on the Pt surface leads to a high production of C_2H_4. Most of the surface oxygen goes to H_2O; this leads to a rapid C buildup on the surface that blocks sites and inhibits C_2H_4 decomposition (Eq. 13).

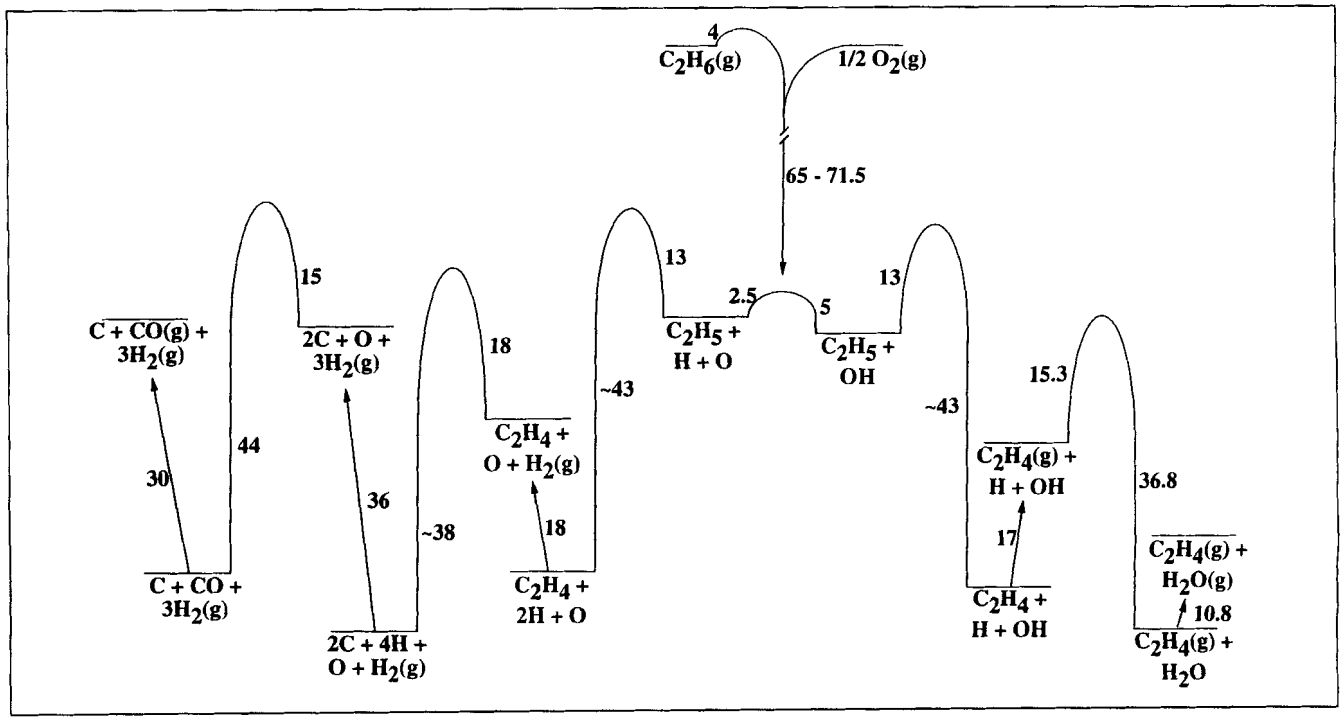

Figure 7. Potential energy diagram for the C_2H_6 partial oxidation and oxidative dehydrogenation system at low coverages and high temperatures on Pt surfaces; all species are surface species unless otherwise noted.

Reaction Temperature

The model assumes isothermal operation at some particular temperature where experimentally the reactor operates near the adiabatic reaction temperature. In the limit of no thermal conductivity along the length of the catalyst, the reaction temperature may vary substantially along the length of the catalyst as the reaction progresses. Monolithic catalysts, however, have high thermal conductivity that leads to high rates of heat transfer and nearly isothermal operation.

Figure 8 shows the effect of reaction temperature on the model predictions of selectivities and conversion. This indicates that lower reaction temperatures favor C_2H_4 selectivity, while higher reaction temperatures lead to higher conversion. So, for this case, the optimum C_2H_4 yield (yield = selectivity $\times$ conversion) occurs at a reaction temperature of $\sim$ 1,250 K. This temperature is very close to the adiabatic reaction temperature observed experimentally under these reaction conditions (Huff and Schmidt, 1993).

Two abrupt changes in the selectivities are predicted as the reaction temperature is varied. At $\sim$ 900 K, the selectivity to H_2O begins to decrease with increasing temperature. This appears to be the lower temperature bound for significant steam reforming (Eq. 15). The transition is accompanied by a leveling in the selectivities to C_2H_4 and CO. At $\sim$ 1,250 K, the ethane conversion goes to completion and the product distribution shifts to more CO and H_2 and less C_2H_4 and H_2O than seen at the lower temperatures. It appears that high temperature creates additional vacancies through high rates of desorption. These vacancies lead to decomposition of adsorbed C_2H_4 to C and H, which ultimately leads to increased CO and H_2 production through reaction with H_2O (the O coverage at temperatures $>$ 1,100 K is very low).

Model Predictions

Since the model reproduces the experimental data fairly well, we can use it to learn more about the reaction system behavior. We can thus use the model to probe reaction conditions that are difficult to probe experimentally.

Dependence on residence time

By changing the flow rate of the reactants, the residence time τ in the catalyst changes. High flow rates correspond to short residence times. In Figure 9, the reactant flow rate has been varied over a 1-cm Pt catalyst.

There is a transition region in the product selectivities between 2.0 and 5.0 slpm from high conversion and lower C_2H_4 selectivity to lower conversion but higher C_2H_4 selectivity at higher flow rates (shorter τ). At the slower flow rates, C_2H_6 is completely consumed and the steam-reforming reaction begins to dominate the product distribution, as discussed in the previous section. At flow rates $>$ 2 slpm, C_2H_6 breakthrough occurs because there is insufficient time for the C_2H_6 to adsorb and react. This corresponds well with experimental results (Huff and Schmidt, 1993).

Another way to vary the residence time is by altering the length of the catalyst. This can be done easily with the model,

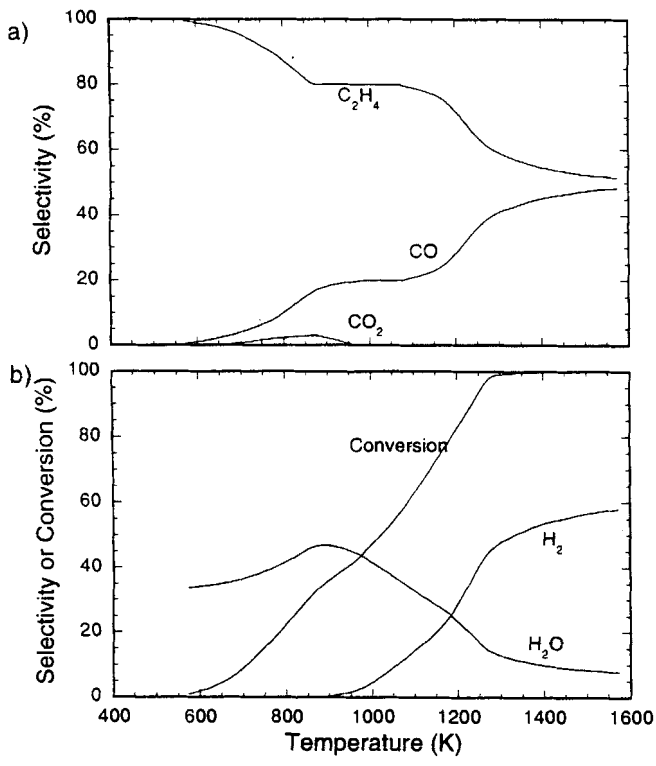

Figure 8. Model predictions of selectivities and conversion as a function of the reaction temperature.

The solid curves represent the model predictions on Pt ($C_2H_6/O_2 = 1.65$, 20% N_2, 5 slpm).

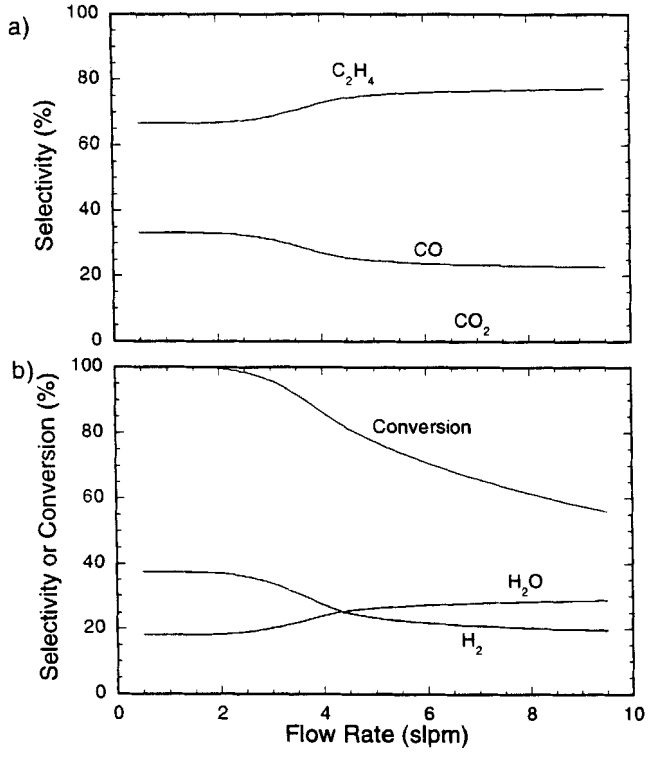

Figure 9. Model predictions of selectivities and conversion as a function of the reactant flow rate in slpm.

The solid curves represent the model predictions on the Pt ($C_2H_6/O_2 = 1.65$, 20% N_2, 1.4 atm, 1 cm length, 900°C).

while experimentally it requires fabrication of many monolith sizes. Model results from variable catalyst lengths reproduce the results shown in Figure 9 for variable flow rate, indicating that the critical variable is the residence time.

Dependence on reaction pressure

In industrial practice, it is common to operate a process at elevated pressures to improve the reactor throughput among other practical concerns. Experimentally, it is dangerous and expensive to operate at elevated pressures, but we can use the model to predict what will happen at pressures other than 1.4 atm, where all of the experiments were conducted (Huff and Schmidt, 1993).

Figure 10 shows the variation in selectivities and conversion as a function of the total reactor pressure for ethane oxidation in O_2 (20% N_2) at a C_2H_6/O_2 ratio of 1.65 at a total flow rate of 5 slpm. Since the total flow rate is held constant, the catalyst contact time increases as the pressure increases.

The model predicts that, as pressure increases, the C_2H_4 and H_2O selectivities both increase while the conversion decreases. The maintenance of C_2H_4 yield is extremely good for the potential industrialization of this process. It is likely that the higher pressures lead to higher coverages on the surface, which (1) decreases the activity of the catalyst and ethane conversion, and (2) limits the availability of vacant sites for the decomposition of C_2H_4 leading to a higher C_2H_4 selectivity. These model results agree well with the limited experiments that have been done at different reaction pressures (Dietz and Schmidt, 1995).

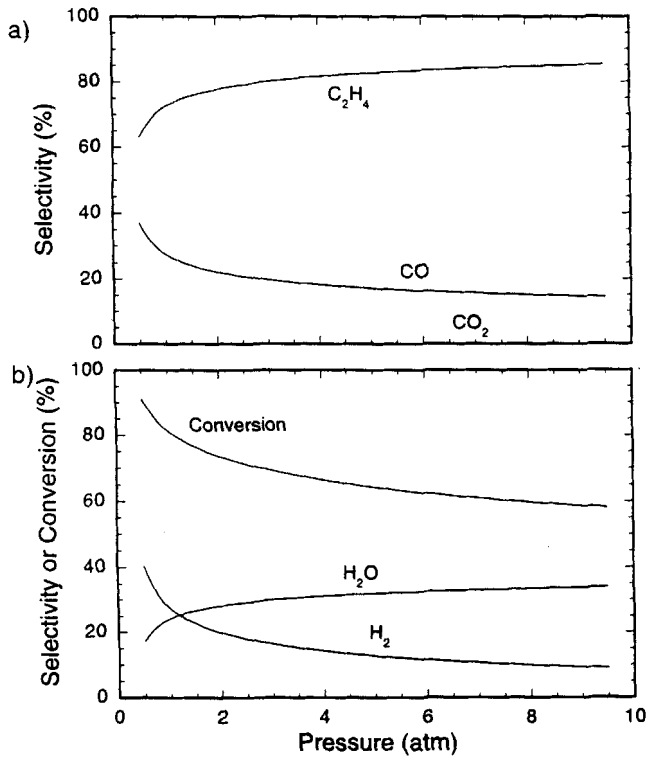

Figure 10. Model predictions of selectivities and conversion as a function of the total reaction pressure.

The solid curves refer to a Pt catalyst ($C_2H_6/O_2 = 1.65$, 20% N_2, 5 slpm, 1 cm length, 900°C).

It is important to realize that this simple model does not address many of the concerns that can become significant at elevated pressures. The flammability limits of mixtures of C_2H_6 and O_2 widen at higher pressures. This suggests that homogeneous reactions can play a more significant role in the mechanism at higher pressures than they play near atmospheric pressure. The model does not include the possibility of these homogeneous reactions or the possibility of dimerization reactions.

$$2C_2H_4(g) \rightarrow C_4H_8(g), \tag{49}$$

$$2C_2H_4 \rightarrow C_4H_8 \rightarrow C_4H_8(g), \tag{50}$$

which become more important at higher pressures.

Applicability of the Model

There were several simplifying assumptions made to create a workable computer model of the ethane oxidation system. Since these assumptions limit the applicability of this model, the assumptions must be reviewed before applying the model to real experiments or industrial conditions.

Kinetic parameters

When the rate parameters listed in Table 1 were available from the literature, they were measured at specific conditions, often on single crystal surfaces and always at low coverages. This limits the model applicability to low coverage conditions that can usually be assumed at high operating temperatures. The only species that are present at appreciable coverages are C and CO, as shown in Figure 2.

These UHV experiments were conducted in the absence of competing adsorbates. Even at low coverages, adsorbate–adsorbate interactions are likely and may potentially alter many of the activation energy barriers. For example, any given surface reaction may behave differently in the presence of adsorbed CO or C. In fact, many of the reactions may be catalyzed by carbon, which will invalidate the given kinetics.

The preexponentials that were unavailable in the literature were treated as adjustable parameters used to fit the model to the known ethane oxidation data (Huff and Schmidt, 1993). Since there were five "adjustable" parameters in the basic model and seven "adjustable" parameters in the extended model, it is likely that combinations other than the ones listed in Table 1 would also fit the experimental data. This fact introduces the possibility of large errors if the model is applied to ethane oxidation under reaction conditions far outside the realm of the fitting procedure.

Reaction mechanism

The model is a simplified depiction of the ethane-oxidation system. It neglects many secondary reactions that can have a large effect on the reaction products. These secondary reactions include ethylene dimerization to form butylene (Eq. 50), methane formation from adsorbed ethyl,

$$C_2H_5 \rightarrow CH_4 + CH \rightarrow CH_4(g) + C + H, \tag{51}$$

CO disproportionation,

$$2CO \leftrightarrow CO_2(g) + C, \tag{52}$$

and steam reforming of C_2H_4,

$$C_2H_4 + 2H_2O \rightarrow 2CO + 4H_2. \tag{53}$$

The model also assumes that several steps are irreversible. Ethylene is not allowed to readsorb and further react or decompose, something that is almost certainly occurring experimentally. All of these reactions will reduce the experimentally or industrially achieved C_2H_4 selectivity below the value predicted by the model.

The model also assumes a purely heterogeneous mechanism. At the reaction temperatures experimentally observed (800–1,100°C) (Huff and Schmidt, 1993), homogeneous reactions undoubtedly have nonzero rates. However, with the limited reaction time ($\tau < 10$ ms) we believe that the contribution of these homogeneous reactions is small relative to the catalyzed heterogeneous reactions. Recent experimental work indicates that at 1,000°C with reaction times of ~ 5 ms, conversions in the absence of noble metal catalyst are $< 20\%$ (Goetsch and Schmidt, 1996). The actual mechanism may be a combination of gas-phase reactions, surface reactions, and surface-initiated gas-phase radical reactions. This model only considers the contribution of surface reactions and predicts the data relatively well. This suggests that under the specific conditions presented in Figures 3–5, surface reactions dominate the other possible reaction mechanisms. This may not be the case at different reaction conditions such as higher pressure, higher temperature, or longer reaction time.

Reaction temperature

In this model, we assumed isothermal operation. This assumption requires that the catalyst bed be highly conductive. In the case of monolithic catalyst, this is a reasonable assumption. Heat is distributed very rapidly through the monolith by its high thermal conductivity. Other support materials (i.e., the packed bed) lack this high thermal conductivity, and the isothermal operation assumption is invalid.

Summary

In the basic model, we use a 23-step elementary-step mechanism to describe ethane oxidation over Pt catalysts. We are able to do a surprisingly good job of reproducing known experimental data (Huff and Schmidt, 1993). Of the 46 rate parameters used to model this system, 41 were obtained from independent measurements and the remaining 5 preexponentials were used as fit parameters and varied within physically meaningful boundaries.

Our ability to reproduce experimental data with the basic model and predict reasonable product distributions at various reaction conditions suggests that the mechanism proposed here is a fairly accurate depiction of the chemical system within this rather narrow range of applicability. With only five rate parameters obtained from this work, the basic model is well grounded in established kinetic data, and is therefore quite powerful for studying this reaction in this type of reactor under these reaction conditions.

With the extended model, on the other hand, we do an even better job of matching the experimental data, suggesting that steam reforming is indeed an important part of this reaction system. However, kinetic parameters for the steam-reforming reaction have not been independently measured elsewhere, so the extended model has seven adjustable rate parameters. This reduces the predictive ability of this version of the model since slight changes in one or more of the rate parameters can predict vastly different results.

This model contains several simplifying assumptions, and thus is not the last word in describing ethane oxidation on Pt surfaces. However, we consider it a benchmark for future, more refined models that should possess more reliable applicability. This model will become more robust as independently measured rate parameters become available, and as more detailed ways of accounting for heat and mass transfer within the complex catalyst geometry are incorporated.

Acknowledgment

This research was supported in part by the National Science Foundation under grant CTS-9311295.

Notation

E_{Act} = activation energy for reaction i
F = total molar flow rate
$F_{i,o}$ = molar flow rate of species i at the inlet
F_o = total molar flow rate at the inlet
k_{ai} = rate coefficient for the adsorption of species i
k_{di} = rate coefficient for the desorption of species i
k_i = rate coefficient for reaction i
$k_{i,o}$ = preexponential for the rates expression for reaction i
N_{av} = Avogadro's number
P = reactor pressure
R_g = gas constant
$S_{k,i}$ = sensitivity of the model to the value of the preexponential for reaction i
$S_{E,i}$ = sensitivity of the model to the value of the activation energy for reaction i
S_i = selectivity of formation of species i
T_g = gas temperature
T_o = initial feed temperature
T_s = autothermal surface temperature
v_o = linear velocity of the gases at the feed conditions
x = length along the bulk catalyst axis
z = length along the axis of the catalyst pore

Greek letters

$\Delta H^\circ_{f\,298}$ = heat of formation at STP
ΔH_i = heat of reaction i at the reaction temperature
ν_{ij} = stoichiometric coefficients for species i in reaction j

Literature Cited

Berlowitz, P., C. Megiris, J. B. Butt, and H. H. Kung, "The Activity of Pd(110) for Methanol Synthesis," *Langmuir*, **1**, 206 (1985).
Campbell, C. T., G. Ertl, H. Kuipers, and J. Segner, "A Molecular Beam Study of the Catalytic Oxidation of Carbon Monoxide on a Pt(111) Surface," *J. Phys. Chem.*, **73**, 5862 (1980).
Campbell, C. T., G. Ertl, H. Kuipers, and J. Segner, "A Molecular Beam Investigation of the Interactions of CO with a Pt(111) Surface," *Surf. Sci.*, **107**, 207 (1981).
Carter, E. A., and B. E. Koel, "A Method for Estimating Surface Reaction Energetics: Application to the Mechanism of Ethylene Decomposition on Pt(111)," *Surf. Sci.*, **226**, 339 (1990).
Dietz, A. G., and L. D. Schmidt, "Effect of Pressure on 3 Catalytic

Partial Oxidation Reactions at Millisecond Contact Times," *Catal. Lett.*, **33**(1), 15 (1995).
Fisher, G. B., and J. L. Gland, "The Interaction of Water with a Pt(111) Surface," *Surf. Sci.*, **94**, 446 (1977).
Gland, J. L., F. Zaera, D. A. Fischer, R. G. Carr, and E. B. Kollin, "Ethylidyne Formation Rates on the Pt(111) Surface," *Chem. Phys. Lett.*, **151**, 227 (1988).
Goetsch, D. A., and L. D. Schmidt, "Microsecond Catalytic Partial Oxidation of Alkanes," *Science*, **271**, 5255, 1560 (1996).
Hickman, D. A., and L. D. Schmidt, "Steps in CH_4 Oxidation on Pt and Rh Surfaces: High Temperature Reactor Simulations," *AIChE J.*, **39**, 1164 (1993), and references therein.
Huff, M., and L. D. Schmidt, "Ethylene Formation by Oxidative Dehydrogenation of Ethane over Monoliths at Very Short Contact Times," *J. Phys. Chem.*, **97**, 11815 (1993).
Kang, D. B., and A. B. Anderson, "Adsorption and Structural Rearrangement of Acetylene and Ethylene on Pt(111): Theoretical Study," *Surf. Sci.*, **155**, 639 (1985).
Matsushima, T., "Dissociation of Oxygen Admolecules on Rh(111), Pt(111), and Pd(111) Surfaces at Low Temperatures," *Surf. Sci.*, **157**, 297 (1985).
McCabe, R. W., and L. D. Schmidt, "Binding States of CO and H_2 on Clean and Oxidized Pt(111)," *Surf. Sci.*, **65**, 189 (1977).
Mohsin, S. B., M. Trenary, and H. J. Robots, "Kinetics of Ethylidyne Formation on Pt(111) from Time Dependent Infrared Spectroscopy," *Chem. Phys. Lett.*, **154**, 511 (1989).
Ogle, K. M., J. R. Creighton, S. Akhtar, and J. M. White, "The Formation and Decomposition Kinetics of Alkylidynes on Pt(111)," *Surf. Sci.*, **169**, 246 (1986).
Song, Y., L. J. Velenyi, A. A. Leff, W. R. Kliewer, and J. E. Metcalfe, "Steamless Pyrolysis of Ethane to Ethylene," *Novel Production Methods for Ethylene, Light Hydrocarbons, and Aromatics*, L. F. Albright, B. L. Crynes and S. Nowak, eds., Marcel Dekker, New York, p. 319 (1992).
Williams, W. R., C. M. Marks, and L. D. Schmidt, "Steps in the Reaction $H_2 + O_2 \rightarrow H_2O$ on Pt: OH Desorption at High Temperatures," *J. Phys. Chem.*, **96**, 5922 (1992), and references therein.
Windham, R. G., M. E. Bartram, and B. E. Koel, "Coadsorption of Ethylene and Potassium on Pt(111). 1. Formation of a π-bonded State of Ethylene," *J. Phys. Chem.*, **92**, 2862 (1988).
Witt, P. M., and L. D. Schmidt, "Effect of Flow Rate on Partial Oxidation of Methane and Ethane," *J. Catal.*, in press (1996).

Manuscript received Feb. 13, 1996, and revision received June 10, 1996.